Solid-State Electronics, 1977, Vol. 20, pp. 77–89. Pergamon Press. Printed in Great Britain

A REVIEW OF SOME CHARGE TRANSPORT PROPERTIES OF SILICON†

C. JACOBONI, C. CANALI, G. OTTAVIANI and A. ALBERIGI QUARANTA
Istituto di Fisica dell'Università di Modena, 41100 Modena, Italy

(*Received* 18 *March* 1976; *in revised form* 12 *July* 1976)

Abstract—This paper reviews the present knowledge of charge transport properties in silicon, with special emphasis on their application in the design of solid-state devices. Therefore, most attention is devoted to experimental findings in the temperature range around 300 K and to high-field properties. Phenomenological expressions are given, when possible, for the most important transport quantities as functions of temperature, field or impurity concentration. The discussion is limited to bulk properties, with only a few comments on surface transport.

NOTATION

- A parameter in phenomenological equation
- B parameter in phenomenological equation
- C parameter in phenomenological equation
- D, D_{ik} diffusion coefficient
- D_e electron diffusion coefficient
- D_E Einstein diffusion coefficient
- $D_\parallel$ diffusion coefficient parallel to **E**
- $D_\perp$ diffusion coefficient perpendicular to **E**
- $e(b)$ electron in bulk
- $e(s)$ electron on surface
- $\mathbf{E}$ electric field
- E_c parameter in phenomenological equation
- F parameter in phenomenological equation
- f distribution function
- $h(b)$ hole in bulk
- $h(s)$ hole on surface
- $\hbar\omega_0$ optical phonon energy
- I electric current
- $\mathbf{j}, j_i$ current density
- K Boltzmann constant
- $\mathbf{k}, k_i$ carrier wave-vector
- m carrier effective mass
- m_l longitudinal effective mass
- m_t transverse effective mass
- N impurity concentration
- n carrier concentration
- N_{ref} parameter in phenomenological equation
- n_{inv} carrier concentration in inversion layer
- q carrier charge
- $\mathbf{r}, x_i, x$ position
- R penetration range of radiation
- S parameter in phenomenological equation
- $SCLC$ space charge limited current
- T temperature
- ToF time of flight
- T_R transit time
- t time
- $\mathbf{v}$ velocity
- V electric potential
- $v(b)$ bulk drift velocity
- $v(s)$ surface drift velocity
- v_d drift velocity
- v_e electron drift velocity
- v_h hole drift velocity
- v_s saturation drift velocity
- v_{se} electron saturation drift velocity
- v_m parameter in phenomenological equation
- v^* parameter in phenomenological equation
- v_x x component of drift velocity
- W sample thickness
- α parameter in phenomenological equation
- β parameter in phenomenological equation
- γ parameter in phenomenological equation
- κ dielectric constant
- Θ parameter in phenomenological equation
- μ mobility
- μ_e electron mobility
- μ_h hole mobility
- μ_{inv} mobility in inversion layers
- μ_{min} parameter in phenomenological equation
- μ_{max} parameter in phenomenological equation
- μ_0 pure-lattice mobility
- ρ resistivity
- $\langle\epsilon\rangle$ mean carrier energy
- ϵ_0 equilibrium mean carrier energy
- τ_ϵ energy relaxation time
- τ_m momentum relaxation time
- τ_s time to reach steady state condition

1. INTRODUCTION

For several decades the electronics industry has made increasing use of semiconductor materials in the manufacture of solid-state components. To date, most of these devices have been made of silicon, and, as a result, a great deal of research has gone into the physical properties of this material, in order to improve production and design processes.

Transport phenomena play a fundamental role in solid-state devices and therefore, since the fifties, research has largely been devoted to the study of electron- and hole-transport properties. Furthermore, the progressive refinement of electronic technology, mainly related to high-speed/high-frequency devices, has required a corresponding increase in our knowledge of transport quantities, such as drift velocity, v_d, and diffusion coefficient, D, as functions of different parameters (electric field E, temperature T, impurity content N and crystallographic direction).

Knowledge of the linear response regime (Ohmic region) is not sufficient for the task in hand, hence intensive study has been made of the high-field region (hot-electrons), where the electron gas, heated up by the intense field strength, is no longer in equilibrium with the crystal lattice.

†Partially supported by Consiglio Nazionale delle Ricerche, Italy.

The aim of the present paper is to present a review of the most important recent findings regarding electron- and hole-transport properties in silicon, with special emphasis on their application in the design of solid-state devices.

Although for an important class of solid-state devices (e.g. MOS), surface conduction plays a fundamental role, we shall confine ourselves in this paper primarily to bulk properties. Most attention will be devoted to experimental findings, just enough theoretical background, being given to illustrate the fundamentals of charge transport in silicon. Furthermore, we shall give some phenomenological expressions for important quantities to be used in practical computations.

In Section 2 the current theoretical model for transport in silicon is briefly summarized. Section 3 contains a review of the experimental techniques used for the determination of the most important transport quantities, namely, v_d and D. The experimental knowledge of these quantities to date is presented in Section 4. Analytical fits of some of the experimental results are reported in Section 5, while Section 6 sums up the present state of the art and comments on its possible evolution in the near future.

2. THE THEORETICAL MODEL

The response of charge carriers inside a crystal to an external driving agent such as an electric field or a concentration gradient is described by the well-known transport Boltzmann equation, solution of which yields the distribution function $f(\mathbf{r}, \mathbf{v}, t)$ of the charge carriers and therefore the transport quantities of interest[1–4].

Under appropriate conditions, the current density is given by the simple drift-diffusion equation:

$$\mathbf{j} = qn\mu\mathbf{E} + qD\nabla n, \qquad (1)$$

where q is the electronic charge, n the carrier concentration, $\mathbf{E}$ the electric field and μ and D the mobility and the diffusion coefficient, respectively.

The transport parameters μ and D are related to each other, in thermal equilibrium, by the Einstein relation, $D = \mu KT/q$, and can be obtained, in principle, by solving the Boltzmann equation linearized with respect to external forces[1, 4].

Equation (1), however, cannot be applied if we exceed the limits of the linear response regime; at high applied fields the drift velocity is no longer a linear function of E (i.e. μ in the eqn (1) is no longer a constant) and the Einstein relation is no longer valid. In this case, the transport equation must be solved without linearization in the applied field[3–5].

To set up the Boltzmann equation, knowledge is required of the band structure and the scattering mechanisms which govern the dynamics of the carriers inside the crystal.

The conduction band of Si[6, 7] contains six equivalent minima (valleys) along the $\langle 100\rangle$ crystallographic directions; other relative minima are much higher in energy and are not involved in transport processes[8]. The six lowest valleys are ellipsoidal in shape and are centered at about $0.8k_{\max}$ ($k_{\max}$ being the limit of the Brillouin zone) and elongated along the $\langle 100\rangle$ directions. Therefore in each valley electrons exhibit a longitudinal effective mass m_l larger than the transverse effective mass m_t.

The valence band[9, 10] consists of two sub-bands, degenerate at $\mathbf{k} = 0$, and of a third band which is split off by 0.044 eV. Owing to the energy separation and to the low density of states, this third band makes only a small contribution to the hole transport[11]. The two highest sub-bands are non parabolic and are warped, so that the effective mass results to be a function of both the energy of the hole and the direction of its wave-vector.

Charge carriers undergo scattering processes mainly from acoustic and optical phonons and from ionized impurities. Electron transitions can be either intravalley, if both the initial and the final states are in the same valley, or intervalley if they lie in different valleys. Analogously, hole transitions can be intraband or interband.

The importance of ionized impurity scattering depends, of course, upon the impurity content in the crystal. However, owing to the Coulomb nature of this scattering, its importance is in general dominant at the lowest electron energies, that is at low temperatures and low applied electric fields.

As regards phonon scattering, optical or intervalley transitions are controlled by a characteristic energy (typically equivalent to a few hundred degrees Kelvin); therefore, they become important at the higher temperatures; while acoustic modes are more important at the lower temperatures.

The solution of the Boltzmann equation in the non-linear regime (non Ohmic response) has been attempted with both analytical and numerical techniques[5, 12–14]. The most important analytical approximation is based on the "*a priori*" assumption of a heated Maxwellian distribution function. Even though this approximation has often been found to be far from correct[4, 8, 13], it has served to illustrate, and provided a terminology for, the hot-electron problem.

Of the numerical techniques, the most widely used and the most direct is the Monte Carlo method[8, 13], by which a possible history of a single particle is stochastically simulated. When simulation is carried on for a sufficient time, the history of the particle is a correct representation of the overall electron gas. Figure 1 illustrates the principles of Monte Carlo simulation.

3. THE EXPERIMENTAL TECHNIQUES

The first determinations of charge carrier mobility in semiconductors were based on the combined measurements of conductivity and Hall effect in samples with low applied fields. The Haynes–Shockley experiment[15] of 1949 also allowed a determination of the diffusion constant, thus verifying the Einstein relation in the Ohmic region.

Later 1951 the conductivity technique was applied to measure the deviation from the Ohmic response of hot carriers with high applied fields[16–19]. Special care needs to be exercised in its application, however, if variations in the electric field are not to cause variations in carrier density, owing to ionization or injection at the contacts.

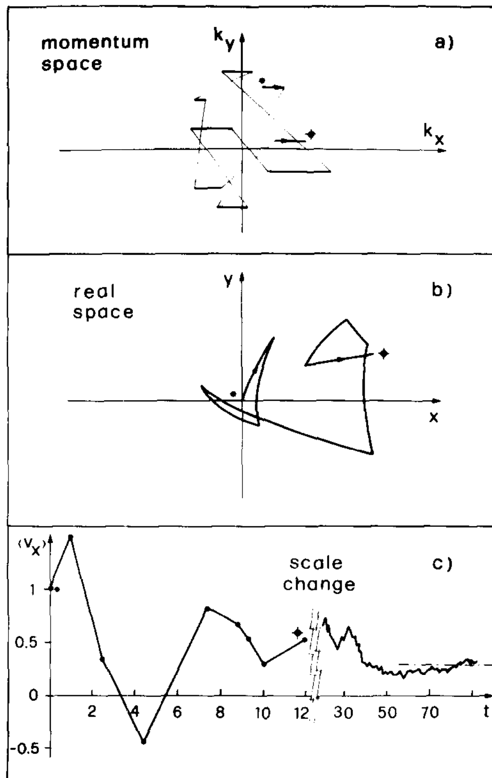

Fig. 1. The principles of the Monte Carlo method; for simplicity a two-dimensional model is considered here.

Part (a) of the figure shows the simulation of the sampling particle, in the momentum space, subject to an accelerating force (field) oriented along the positive x direction. The heavy segments are due to the effect of the field during free flights, while light lines represent discontinuous variations of $\vec{k}$ due to scattering processes.

Part (b) shows the path of the particle in real space. It is composed of eight fragments of parabolas corresponding to the eight free flights in part (a) of the figure.

Part (c) shows the average velocity of the particle obtained as a function of simulation time. The left section of the curve ($t < 12$) is obtained by the simulation illustrated in the parts (a) and (b) of the figure. The horizontal dot-dashed line represents the "exact" drift velocity obtained with a very long simulation time.

Special symbols indicate corresponding points in the three parts of the figure (∗ is the starting point). All units are arbitrary.

To overcome these difficulties, alternative techniques have been used, such as the microwave[20–24] and the time-of-flight[25–29] (ToF)† techniques.

Recently, the time-of-flight[27, 30, 31] noise[32, 33] and geometrical[34] (see below) techniques were used to measure the diffusion coefficients as a function of the applied field.

3.1 *Drift-velocity measurements*

As seen above, there are three basic experimental techniques for the determination of $v_d(E)$:

(a) conductivity technique;
(b) microwave technique;
(c) time-of-flight technique (ToF).

The first measurements of $v_d(E)$ were performed by means of the conductivity technique mainly on account of its simplicity. The microwave technique has also been widely applied, although it is difficult to deduce v_d from the experimental results. These first two techniques have certain drawbacks in common:

(i) they can only be applied to materials with relatively low resistivity;
(ii) they give an indirect measurement of v_d;
(iii) only the drift velocity of the majority carriers can be measured.

(a) *The conductivity technique* is based on a measurement of the current density $j(E)$ in an extrinsic semiconductor sample;

$$j(E) = nqv_d(E), \qquad (2)$$

where n and q are the carrier density and the charge, respectively. Once n has been determined by the Hall-effect measurement (at low fields) the drift velocity can be determined, provided n remains constant, independently of E. It must be noted, however, that n can be affected by changes in E as a result of Joule heating, carrier injection at the contacts or impact ionization. The first two effects are usually avoided by applying very short pulses to samples of special geometry[16, 17]; however, this requires low-resistivity material to minimize the relative contribution of the displacement current. Impact ionization can be avoided only by keeping the field strength sufficiently low. In any event, avalanche multiplication as well as carrier injection have been taken into account in more refined experiments[35–38].

(b) *The microwave technique* can be applied in two essentially different ways: (i) the charge carriers are heated up by a pulsed electric field, and their mobility is determined through a measurement of the attenuation of a low microwave field[22, 23]. (ii) The charge carriers are heated up by a large pulsed microwave field, and their mobility is determined with the aid of a low d.c. electric field[24].

The application of only a strong microwave field is less common[39]; as stated above, the microwave technique at high fields, yields results which are difficult to interpret and is today rarely used for the determination of v_d.

(c) *The time-of-flight* technique consists of the measurement of the time T_R taken by the charge carriers, generated by an appropriate radiation, to travel across a region of thickness W under the influence of an electric field E, ($v_d = W/T_R$). The ionizing radiation must create charge pairs in a period of time much shorter than T_R and in a region of thickness R much less than W. Owing to the electric field, one type of carrier is collected after having travelled only a distance $R \ll W$, while the other is swept towards the opposite contact, inducing a current pulse of duration T_R at the contacts. It is therefore evident that with the ToF technique the $v_d(E)$ characteristics can be obtained in the same sample for both type carriers.

For the application of this technique the following conditions must be fulfilled: (i) the material must have a sufficiently high resistivity to keep Joule heating negligible, and afford a dielectric relaxation time $\rho\epsilon$ longer than T_R[40]; (ii) the mean lifetime of the carriers must not be short compared with T_R[29].

†This technique has been called the transient current technique (TCT) (Ref. [29]).

It may be noted that the ToF technique is similar to the Haynes–Shockley technique. However, the Haynes–Shockley technique allows measurements only on minority carriers in low-resistivity materials ($\rho\epsilon \ll T_R$), while the ToF technique enables the drift velocity of both carrier types to be measured in the same sample, providing high resistivity material ($\rho\epsilon \gg T_R$) is used.

Figure 2 shows some experimental results for electron- and hole-drift velocity, as a function of field strength, obtained with the different techniques discussed above. The results of the different experiments are in satisfactory agreement with each other.

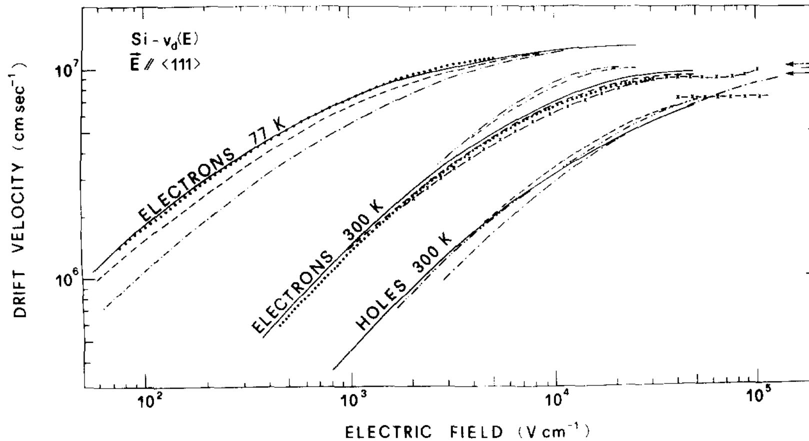

Fig. 2. Comparison of some experimental results, obtained with different techniques, on electron- and hole-drift velocities as functions of electric field E applied parallel to a ⟨111⟩ crystallographic direction.

Holes, $T = 300$ K: (——) Canali *et al.*[28], ToF; (– – –) Norris and Gibbons[26], ToF; (··–··–) Sigmon and Gibbons[30], ToF; (x—x—x) V. Rodriguez *et al.*[35], I(V) in space charge limited current (SCLC) regime; (–·–·–·) Seidel and Scharfetter[37], I(V); (→) extrapolated value for the saturated hole drift velocity by the same authors[37].

Electrons, $T = 300$ K: (——) Canali *et al.*[28], ToF; (—·—) Norris and Gibbons[26], ToF; (– – – –) Sigmon and Gibbons[30], ToF; (··–··) Rodriguez and Nicolet[36], I(V) in SCLC regime; (······) Boichenko and Vasetskii[41], I(V); (–x–x–) A. C. Prior[19], I(V); (- - - →) saturated electron-drift velocity from Duh and Moll[38], I(V) in avalance diodes.

Electrons, $T = 77$ K; (——) Canali *et al.*[28], ToF; (– – – –) Jørgensen *et al.*[42], I(V); (–·–·–) Asche *et al.*[43], I(V); (······) Nash and Holm-Kennedy[44] I(V).

3.2 *Diffusivity measurements*

A knowledge of diffusion processes is useful for a better understanding of charge-transport phenomena and a correct simulation of high-frequency devices.

At low fields the diffusion coefficient D is related to mobility by the Einstein relation; in cubic semiconductors, it is reduced to a scalar quantity. At high fields, however, D becomes a field-dependent tensor[4] which describes the diffusion process parallel and perpendicular to the electric field, with respect to the crystallographic direction of **E**.

Here we assume the definition of D which results from the equation:

$$j_i = q \sum_k D_{ik} \frac{\partial n(\mathbf{r})}{\partial x_k}, \tag{3}$$

where j_i is the i-th component of the electric current density and $n(\mathbf{r})$ is the electron concentration as function of the position **r**.

The difference between the diffusion parallel to and that perpendicular to **E** is due to the nature of the high-field transport process and is greater than the variations caused by changes in the crystallographic direction and which are due to the anisotropy of the material. Therefore, both theoretical and experimental investigations have set out to determine the field dependence of both the longitudinal ($D_\parallel$) and transverse ($D_\perp$) components of D with respect to the electric field, irrespective of its orientation in the crystal.

$D_\parallel$ can be measured by the ToF technique[30, 31] (or by the Haynes–Shockley technique) by observing the difference between the fall and rise times of the current pulse. This difference is caused by the spread of the carriers travelling across the sample and is simply related to the longitudinal diffusion coefficient[27].

Analogously, $D_\perp$ can be obtained by observing the spread of the current perpendicular to the direction of the field. The current is originated by a point excitation on one surface of a Si wafer and is collected on the opposite surface by several electrodes of appropriate geometry[34]. This technique is called as "geometrical technique" in the present paper.

Finally, in recent years both $D_\parallel$ and $D_\perp$ have been related to noise measurements, parallel and perpendicular respectively to the current direction[32, 45].

4. TRANSPORT DATA

In this section we set out the most important transport data available in the literature, with particular reference to temperature, field and impurity-concentration dependences of Ohmic mobilities, drift velocities, and diffusion coefficients. From the discussion of this set of data a complete picture of charge transport in Si should emerge. At the same time, special attention will be paid to high temperatures and field strengths in order to provide as complete a source of information as possible to people

interested in the design and simulation of solid-state devices.

Table 1 contains a recent set of physical parameters for charge transport in Si[8, 11]. As regards these parameters we may recall here a controversy about the phonon energies and coupling strengths which intervene in electron intervalley scattering. The model presented in Table 1 has been obtained by considering that magnetophonon resonance experiments[46] indicate the effect of essentially all existing phonons and by fitting the $v_d(E)$ characteristics in very wide ranges of temperature and field strength. A further improvement of the model has been obtained by considering also band nonparabolicity[47, 48].

Table 1. Set of physical parameters for charge transport in Si used in Refs.[8 and 11]

Density	(ρ)	2.329	g/cm³
Longitudinal sound velocity	(s_l)	9.04×10^5	cm/sec
Transversal sound velocity	(s_t)	5.34×10^5	cm/sec
Dielectric constant	(κ)	11.7	—
Electrons[8]			
Equiv. temp. scatt. f_1	(T_{f1})	210	K
Coupl. const. scatt. f_1	(D_{f1})	1.5×10^7	eV cm⁻¹
Equiv. temp. scatt. f_2	(T_{f2})	500	K
Coupl. const. scatt. f_2	(D_{f2})	3.4×10^8	eV cm⁻¹
Equiv. temp. scatt. f_3	(T_{f3})	630	K
Coupl. const. scatt. f_3	(D_{f3})	4×10^8	eV cm⁻¹
Equiv. temp. scatt. g_1	(T_{g1})	140	K
Coupl. const. scatt. g_1	(D_{g1})	5×10^7	eV cm⁻¹
Equiv. temp. scatt. g_2	(T_{g2})	210	K
Coupl. const. scatt. g_2	(D_{g2})	8×10^7	eV cm⁻¹
Equiv. temp. scatt. g_3	(T_{g3})	700	K
Coupl. const. scatt. g_3	(D_{g3})	3×10^8	eV cm⁻¹
Acoustic def. pot.	(E_1)	9	eV
Transverse effective-mass	(m_t/m_0)	0.1905	—
Longitudinal effective-mass	(m_l/m_0)	0.9163	—
Holes[11]			
Optical phonon temp.	(T_{op})	735	K
Optical def. potential	(D_{op})	5×10^8	eV cm⁻¹
Inverse valence band parameter	(A)	4.27	—
	(B)	0.63	—
	(C)	4.93	—
Acoustic def. pot.	(E_1)	2.2	eV
Split-off energy	(Δ)	0.044	eV
Energy band parameter	(ϵ_0/K)	70	K
	(ϵ_1/K)	130	K
Heavy effective mass	(m_{10}/m_0)	0.55	—
	(m_{11}/m_0)	1.7	—
Light effective mass	(m_2/m_0)	0.2	—

4.1 *Ohmic mobility*

In Fig. 3 the experimental electron mobility μ_e in high-purity[8, 49] and doped silicon[50] is shown as a function of temperature. The theoretical mobility is also given for the pure-lattice case, the agreement between the theoretical and experimental data of high purity material being excellent down to about 50 K. Below this temperature, owing to the effect of impurity scattering, the experimental data are lower than the theoretical curve and differ from each other probably because of different impurity concentrations. The temperature dependence of the lattice mobility is primarily due to acoustic scattering below about 50 K, while above this temperature several

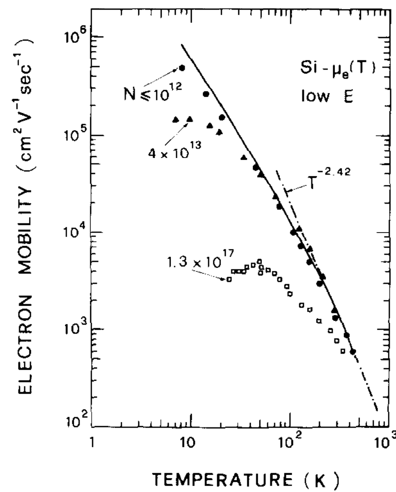

Fig. 3. Ohmic mobility of electrons in silicon as a function of temperature. Closed circles have been obtained[8] with the ToF technique in high purity Si (N ≤ 10^{12} cm^{-3}); closed triangles[49] using photo-Hall effect in high-purity Si; open squares[50] using Hall effect in Si with 1.3×10^{17} cm^{-3} donors. The continuous line indicates the theoretical results for pure-lattice mobility[8]. The dot-dashed line gives a $T^{-2.42}$ dependence of the electron mobility around room temperature (see Table 2).

inter-valley scattering mechanisms become more important[8, 49, 51]. Around room temperature the mobility follows a $T^{-2.42}$ dependence (dot-dashed line).

In the case of sufficiently high impurity concentrations the mobility at low temperature is dominated by Coulomb scattering, and the deviation from the pure-lattice mobility occurs at higher T in less pure material[50].

In Fig. 4 the experimental and theoretical hole mobility μ_h is shown as a function of temperature[11, 50, 52]. The kind of consideration made for electrons also holds well

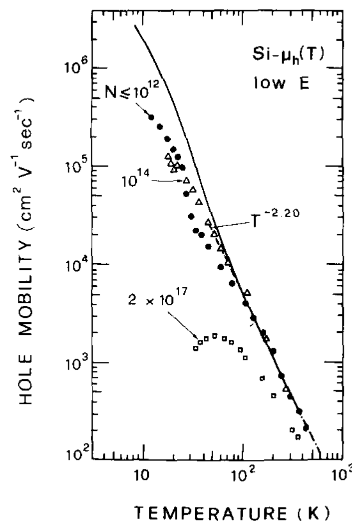

Fig. 4. Ohmic mobility of holes in silicon as a function of temperature. Closed circles have been obtained[11] with the ToF technique in high purity Si; open triangles[52] using Hall effect in high purity Si; open squares[50] using Hall effect in Si with 2×10^{17} cm^{-3} acceptors. The continuous line indicates the theoretical results for pure-lattice mobility[11]. The dot-dashed line gives the $T^{-2.2}$ dependence of the hole mobility around room temperature (see Table 2).

for holes. The temperature dependence of pure-lattice μ_h for $T \leq 100$ K is dominated by acoustic modes, but does not follow the $T^{-1.50}$ dependence due to nonparabolicity of the top of the valence band[11]. Around room temperature μ_h follows a $T^{-2.20}$ law (dot-dashed line) due to optical phonon scattering.

The influence of impurity concentration N on the room temperature mobilities of electrons[53–57] and holes[55, 57, 58] is shown in Figs. 5 and 6, respectively. In both cases, the effect becomes appreciable around $N = 10^{16}$ cm^{-3}, and for $N > 10^{19}$ cm^{-3} μ tends to saturate at a value independent of the impurity concentration. This saturation can be interpreted as being due to the merging of bound states into the conduction band[59].

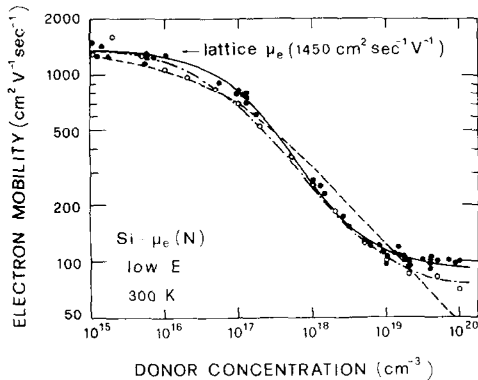

Fig. 5. Electron mobility, μ_e, in silicon at 300 K as a function of impurity concentration. Open and closed circles are the experimental results reported by Irvin[55] and of Mousty *et al.*[56], respectively. The continuous line is the phenomenological best fit (eqn (6)) of Baccarani and Ostoia[53] the broken line the best fit (eqn (7)) of Hilsum[54] the dot-dashed line (eqn (8)) of Scharfetter and Gummel[57] (see Tables 3 and 4).

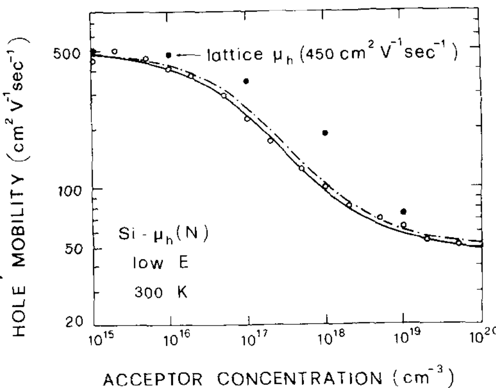

Fig. 6. Hole mobility, μ_h, in silicon at 300 K as a function of impurity concentration. Open circles are experimental results reported by Irvin[55]. Continuous and dot-dashed lines represent the best fitting curves of Caughey and Thomas[58] (eqn (6)) and of Scharfetter and Gummel[57] (eqn (8)), respectively (see Tables 3 and 4).

4.2 *High-field drift velocity*

Extensive measurements and Monte Carlo calculations have been performed recently for both electron[8] and hole[11] drift velocities. Outside the Ohmic, linear region the drift velocity exhibits an anisotropic behaviour with respect to the orientation of the electric field **E** in the crystal[5]. This behaviour consists of different values for v_d obtained with the same field strength and for **E** applied in the main crystallographic directions ⟨111⟩, ⟨110⟩ and ⟨100⟩. For less symmetrical directions, v_d is not even parallel to **E**[60]. Some examples of the anisotropy of v_d are shown in Figs. 7 and 8 for electrons and holes at several temperatures.

In the case of electrons, the anisotropy is due to a repopulation of the valleys: when **E**‖⟨111⟩ the six valleys are equally oriented with respect to **E** and all of them give the same contribution to v_d. When, for example, **E** is parallel to a ⟨100⟩ direction, two valleys exhibit the longitudinal effective mass m_l in the direction of the field, while the remaining four exhibit the transvers mass $m_t < m_l$ [7]. Electrons in transverse valleys respond with a higher mobility, are heated to a greater extent by the field and transfer electrons to the two longitudinal, colder and slower valleys. The net effect is a lower v_d for **E**‖⟨100⟩, as shown in Fig. 7.

A similar anisotropy is present for holes and is due to the two warped and degenerate valence sub-bands resulting in different effective masses for the holes with different **k**[11] and in a lower v_d for **E**‖⟨111⟩, as shown in Fig. 8.

Anisotropy becomes stronger as temperature falls, since the relaxation effects are less effective at lower T. In particular, when $T \leq 45$ K the repopulation of electron valleys may be so rapid with increasing **E** along ⟨100⟩ that a negative differential mobility occurs when E ranges between 20 and 60 V/cm. This effect has been observed as current oscillations[61] and in $I(V)$[62–64] and $v_d(E)$ [8, 65] characteristics.

Whether the electron $v_d(E)$ curves for **E**‖⟨100⟩ and for **E**‖⟨111⟩ join together at the high-field limit is still an open point. Theoretical considerations[66] seem to indicate that a small difference ($\simeq 5\%$) between the two curves should remain; however, this difference is comparable to experimental error to date and the merging of the two curves has been claimed at several temperatures in the experimental results[8, 28]. In the case of holes, both theoretical and experimental results[11] indicate that, up to the highest fields considered (50 KV/cm), no merging occurs.

An overall view of the experimental $v_d(E)$ curves at different temperatures for both electrons (in the ⟨111⟩ direction) and holes (in the ⟨100⟩ direction) is given in Figs. 9 and 10. The most important features to be noted in these data are: (i) a deviation from the Ohmic linear response, which occurs at lower fields as T decreases; (ii) an anomalous behaviour of the $v_d(E)$ curve of holes at low temperatures ($T \leq 30$ K). Owing to nonparabolicity[67] of the valence sub-bands, these curves tend to saturate at intermediate field strengths ($E \simeq 100$ V/cm) and then rise again; (iii) a general tendency of $v_d(E)$ to saturate at the highest fields, an important phenomenon which will be discussed below; (iv) at high fields the $v_d(E)$ characteristics for a given crystallographic direction tend to join together in a temperature independent curve for $T \leq 45$ K. In fact, under the condition of very hot electrons and low lattice

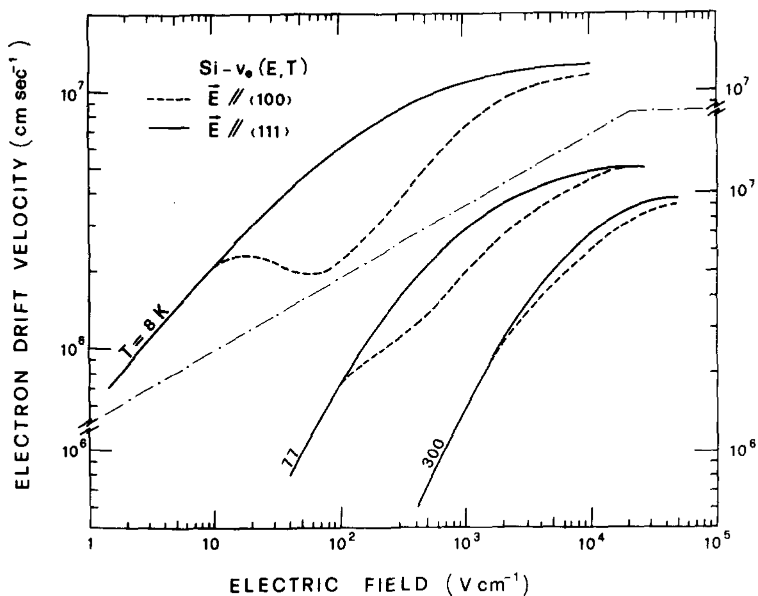

Fig. 7. Experimental results [8, 28] of electron drift velocity as a function of the electric field applied parallel to ⟨111⟩ and ⟨100⟩ crystallographic directions at several temperatures.

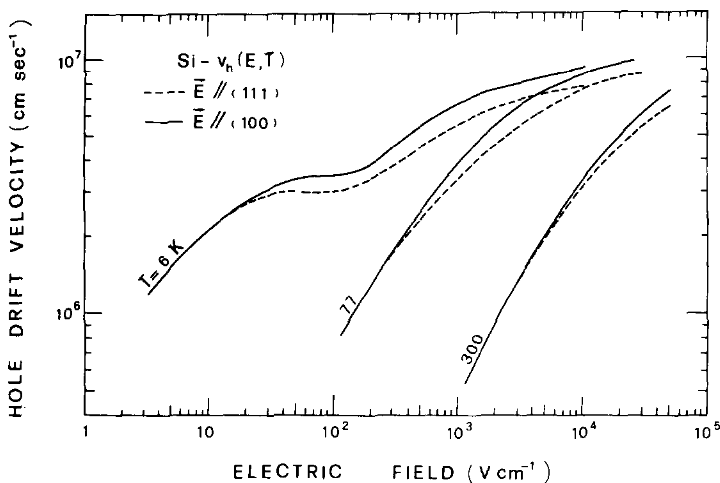

Fig. 8. Experimental results [11, 28] of hole drift velocities as functions of the electric field applied parallel to ⟨111⟩ and ⟨100⟩ crystallographic directions at several temperatures.

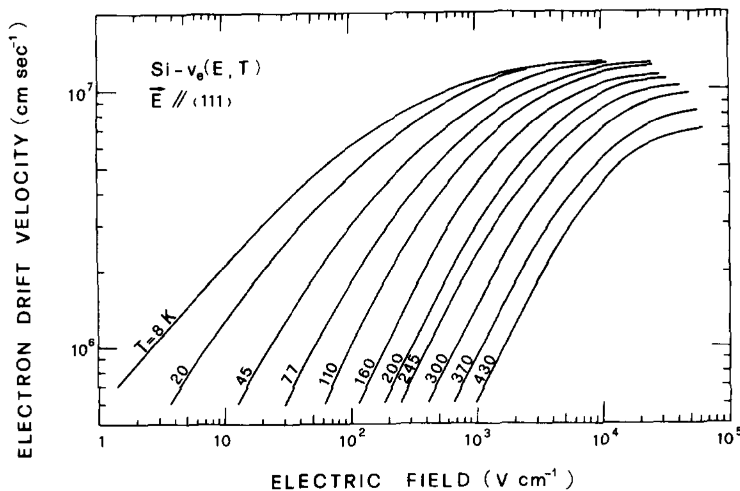

Fig. 9. Experimental electron drift velocity as a function of electric field applied parallel to a ⟨111⟩ crystallographic direction at different temperatures [8, 28].

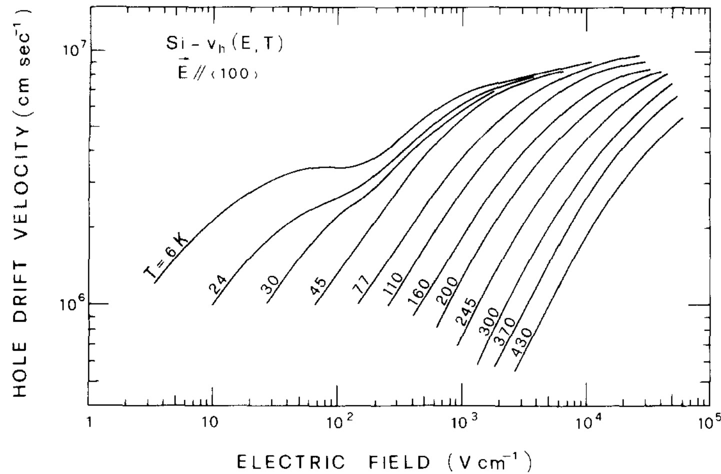

Fig. 10. Experimental hole drift velocity as a function of electric field applied parallel to a ⟨100⟩ crystallographic direction[11, 28].

temperature, the transport phenomenon is dominated by spontaneous phonon emission which is temperature independent (zero point limit).

4.3 *The problem of saturated drift velocity*

From the very beginning of hot-electron investigations[16–18], saturation of the drift velocity in the high-field limit has been considered. The original explanation[17] for this behaviour was based on a very rough physical model in which optical phonon emission was alone considered responsible for limiting the drift velocity in the high-field limit. It was assumed that the carriers emit a phonon as soon as they reach the energy ($\hbar\omega_0$) of the phonon. The saturated drift velocity is then[17, 68, 69]

$$v_s = \left(\frac{8\hbar\omega_0}{3\pi m}\right)^{1/2} \tag{4}$$

where m is the electron effective mass and $\hbar\omega_0$ the optical phonon energy.

Subsequent calculations showed, however, that at very high electric field the transport process is the result of many factors including several phonon dispersion curves, phonon absorption as well as emission, and band nonparabolicity[8, 47]. Therefore, the above eqn (4) must be considered only as a rough evaluation of the saturation of v_d.

On the other hand, for practical purposes of device manufacture, a saturated drift velocity is of particular interest. Thus, in experimental measurements, there is a tendency to consider v_d saturated when, at increasing fields, its variation is so small as to approach constancy, within experimental uncertainty.

In the case of holes, saturation is neither predicted theoretically nor found experimentally. A nearly-saturated drift velocity was observed[37] only at room temperature, and, by extrapolation, v_s should occur at or above fields of 2×10^5 V/cm with a value around 1×10^7 cm/sec (see Fig. 2).

Bearing in mind the above limitations, saturation for electron-drift velocity has been observed at several temperatures with different techniques. Figure 11 indicates the temperature dependence of the saturated electron-drift velocity. For $T \leq 45$ K, v_s is equal to 1.3–1.4 × 10^7 cm/sec, independent of T, this being an effect of the zero-point limit. At higher temperatures, $v_s(T)$ decreases steadily as T increases. At room temperature, v_s is around 1×10^7 cm/sec.

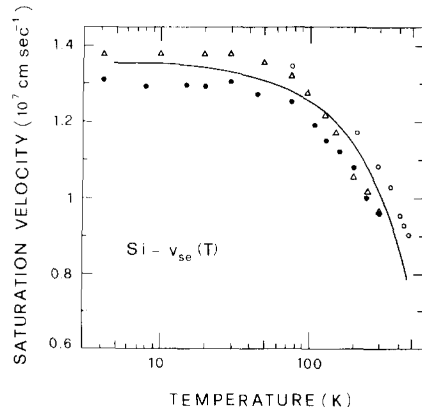

Fig. 11. Temperature dependence of the saturated electron drift velocity obtained experimentally with different techniques: closed circles[8, 28, 70], ToF; open circles[38], I(V) in avalanching diodes; open triangles[36], I(V) in SCLC regime; the latter data have been normalized to 9.6×10^6 cm sec^{-1} at 300 K. The continuous line represents the best fitting curve of eqn (11).

4.4 *Mean energy and energy relaxation time*

The knowledge of carrier mean energy as a function of applied field strength may be useful for having a general picture of charge transport, especially at very high fields, and it may be of relevance in connection with other nonlinear effects such as, for example, avalanche multiplication. Figure 12 reports the electron and hole mean energy at 300 K as a function of field strength obtained with Monte Carlo calculations. For electrons a nonparabolic model has been used and several impurity concentrations considered. For holes the theoretical

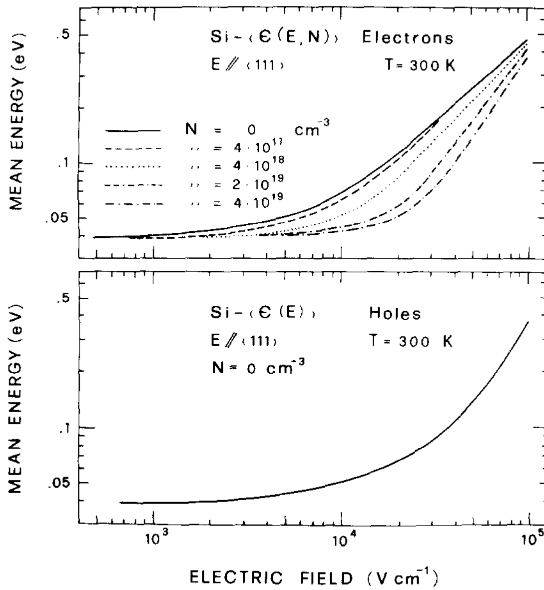

Fig. 12. Theoretical mean energies of electrons (a) and holes (b) as functions of electric field applied parallel to a ⟨111⟩ crystallographic direction at 300 K. For electrons the different curves refer to the indicated impurity concentrations.

analysis is based on a single parabolic and warped band model[71].

From the knowledge of the drift velocity v_d and the mean carrier energy $\langle\epsilon\rangle$ at an electric field E and of the equilibrium mean energy ϵ_0 it is also possible to consider the quantity

$$\tau_\epsilon = \frac{\langle\epsilon\rangle - \epsilon_0}{qv_dE}$$

which can be taken as definition of a phenomenological energy relaxation time τ_ϵ [72, 73], although it has this precise physical meaning only in the limit of low (warm electrons) fields.

Hess and Seeger[74] with the method of harmonic mixing of microwaves have performed an experimental determination of τ_ϵ in the warm carrier region in Si and Ge in the temperature range between 77 and 200 K. τ_ϵ is found to decrease with increasing temperature from τ_ϵ (77 K) $\simeq$ 60 psec to τ_ϵ(150 K) $\simeq$ 16 psec for electrons and from τ_ϵ(77 K) $\simeq$ 30 psec to τ_ϵ(130 K) $\simeq$ 14 psec for holes, in Si.

At 300 K we have found with Monte Carlo calculations that at high fields ($5\cdot10^3 < E < 10^5$ V/cm) τ_ϵ for electrons is almost constant with a value around 0.4 psec. Dargys and Banys[75] determined with a microwave experiment the dependence of τ_ϵ upon field at 77 K. They found a sharp decrease of τ_ϵ from $\tau_\epsilon(E=0) \simeq 65$ psec to $\tau_\epsilon(E = 300$ V/cm$) \simeq 7$ psec followed by a slow variation of τ_ϵ for $300 < E < 2000$ V/cm. The initial sharp decrease of τ_ϵ at increasing fields is due to the heating up of the carriers which in this way gain enough energy to emit optical phonons. At higher lattice temperature, as for example $T = 300$ K, thermal electrons have already energies comparable with that of optical phonons and therefore no sharp decrease of $\tau_\epsilon(E)$ is expected.

In dealing with frequency response of devices, however, it must be considered that two other times, besides τ_ϵ, come into play. They are the momentum relaxation time τ_m and the time τ_s necessary for the charge carriers to give the stationary response to the field. While in general τ_m is much shorter then τ_ϵ, τ_s can be quite longer, thus becoming the discriminating quantity. It depends upon working conditions and therefore it is not possible to make general statements about its value. In a particular case, for electrons in Si at 300 K with zero impurity concentration with $E \simeq 10^5$ V/cm, it has been found $\tau_s \simeq 1$ psec[76].

4.5 *Hot-carrier diffusion*

As mentioned above (Section 3.2), the diffusion coefficient in *Si* indicates its tensor nature at high fields. Therefore, different values are expected for the diffusion coefficient longitudinally ($D_\parallel$) and transversally ($D_\perp$) to **E**.

Figure 13 shows the most recent experimental results of the field-dependence of $D_\parallel$ and $D_\perp$ for electrons in Si at room temperature with $E \parallel \langle 111 \rangle$. The data obtained with noise measurements[33] are in reasonable agreement with time-of-flight results, although the former cover a narrow range of field strength, just outside of the ohmic region. As E increases $D_\parallel$ decreases to about 1/3 of its Ohmic value. This behaviour is in substantial agreement with theoretical Monte Carlo computations which account for band non-parabolicity[31].

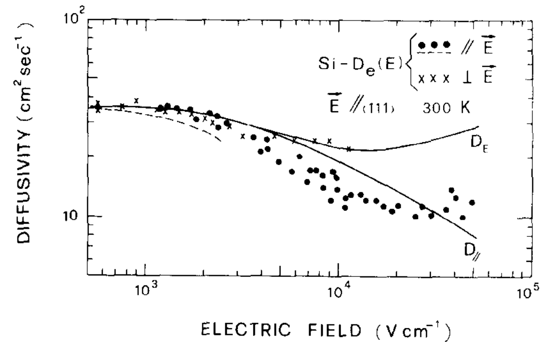

Fig. 13. Diffusion coefficients of electrons in Si at room temperature as a function of field applied parallel to a ⟨111⟩ crystallographic direction. Closed circles show the data of Canali *et al.*[31] for $D_\parallel$, obtained with ToF technique; the broken line, the data of Nougier and Rolland[33] for $D_\parallel$, obtained with noise measurements; crosses, the data of Persky and Bartelink[34] for $D_\perp$, obtained with the geometrical technique (see text). Continuous lines show: a Monte Carlo computation of longitudinal diffusion coefficient, $D_\parallel$, and the diffusion coefficient D_E obtained by using the modified Einstein relation[31]. Both theoretical curves have been obtained with a nonparabolic model.

The results for transverse diffusion show that, as E increases, $D_\perp$ also decreases, but to a lesser extent than $D_\parallel$.

There is a tendency to extrapolate the Einstein relation to high fields by introducing field-dependent mobility, $\mu(E)$, and mean electron energy $\langle\epsilon(E)\rangle$: $D_E(E) = 2/3\,\mu(E)\langle\epsilon(E)\rangle/q$. In some cases, this yields a correct qualitative interpretation of high-field diffusion; for electrons in silicon, however, the process would appear to be more complex (see Fig. 13).

The longitudinal diffusion of holes seems to have a field dependence similar to that of electrons[77]. Data of $D_\perp$ for holes are not as yet available.

4.6 *Surface conductivity*

In recent years, the application of MOS structures in solid-state devices has focused a great deal of attention on the problem of surface conduction. This matter lies beyond the scope of the present work, and we shall confine ourselves to a brief description of its phenomenology, and of the most important models used to explain the experimental data.

Early analyses were generally based on the classical three-dimensional ($3D$) model[78–80] adding to the bulk-scattering mechanisms a partially-diffuse surface scattering. More recently, quantum mechanical models have been developed[80, 81] that consider a potential well so narrow that the motion (perpendicular to the interface) of all the carriers in the surface channel is quantized (electric quantum limit). In this two-dimensional (2D) model the electron-scattering mechanisms common to the 3D model are modified by the 2D nature of the electron dynamics. Other scattering mechanisms are specific for surface conduction, such as scattering from interface charges, surface phonons, and surface roughness.

The main experimental findings are as follows: (i) The surface carrier mobilities, μ_{inv}, in the inversion layers are smaller than the corresponding bulk mobilities and depend upon the applied normal field, or upon the carrier surface-density, n_{inv}, induced in the layer[82–86]. At room temperature, as n_{inv} decreases, electron and hole mobilities increase, and below $n_{inv} \approx 10^{12}\,cm^{-2}$, the mobilities tend to saturate at a value which is about one half of the bulk mobility[83, 84]. However, at lower temperatures this dependence is not monotonic[80, 84], and the reason for this behaviour is still under investigation. (ii) The temperature dependence of μ_{inv} is about $T^{-1.5}$ around room temperature, for both electrons and holes[82–84]. (iii) As the longitudinal field strength increases the surface drift velocity tends to saturate, as in the case of bulk mobility; however, the saturation velocities have been found to be significantly lower than the bulk values (see Fig. 14)[85, 87, 88] and (for electrons) to depend on the surface orientation[87]. (iv) In the case of (110) surfaces, the electron mobility is anisotropic, while in the case of (111) and (100) surfaces it is isotropic, in agreement with symmetry consideration[80, 86, 89].

5. PHENOMENOLOGICAL EXPRESSIONS

In this section we present some analytical expressions that are in good agreement with the most interesting experimental data of charge transport in silicon, and which can be used for numerical calculations in the design of solid-state devices. Several of these analytical expressions have been given in the literature[53, 54, 57, 58, 90–93]. Not all of them will be reported here for obvious reasons of space. As a general comment we should note that a higher range of applicability is of course paid with a more complicated expression and/or a less accurate fitting of the experimental data.

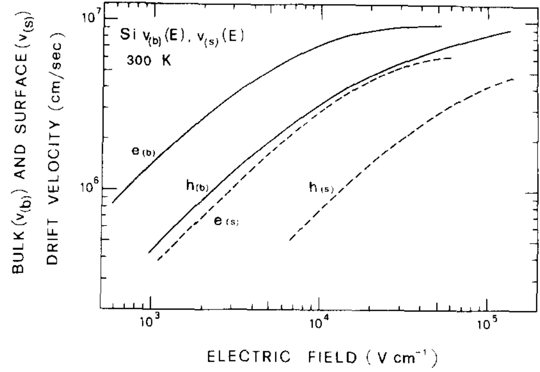

Fig. 14. Continuous lines show the experimental results of electron (e) and hole (h) drift velocities as functions of field strength in bulk [e(b), h(b)] and on surfaces [e(s), h(s)] at room temperature; e(b) and h(b)[28] data were obtained with $\mathbf{E}\|\langle 111\rangle$; e(s)[87] and h(s)[88] on (100) inverted surfaces.

5.1 *Ohmic mobility*

In Figs. 3 and 4 it is shown that, around room temperature, the electron and hole Ohmic mobilities in pure materials have a temperature dependence given by:

$$\mu = AT^{-\gamma} \tag{5}$$

the values of the parameters being given in Table 2.

Table 2. Best-fitting parameters for the temperature dependence of electron and hole ohmic mobilities in high-purity silicon, as given in eqn (5)

	Electrons	*Holes*	*Units*
A	1.43×10^9	1.35×10^8	$cm^2K^{\gamma}\,V^{-1}\,sec^{-1}$
γ	2.42	2.20	—

Several analytical expressions have been given for the Ohmic mobilities of electrons and holes as functions of impurity concentration at room temperature. We report these expressions here and compare them with the experimental data in Figs. 5 and 6. In these figures the continuous lines are calculated with the equation[53, 58]:

$$\mu = \mu_{min} + \frac{\mu_{max} - \mu_{min}}{1 + (N/N_{ref})^{\alpha}}, \tag{6}$$

where N is the impurity concentration, the values of the other parameters being given in Table 3.

Table 3. Best-fitting parameters for the impurity dependence of electron and hole Ohmic mobilities at room temperature, as given in eqn (6)

	Electrons	Holes	Units
μ_{min}	92	47.7	$cm^2\,V^{-1}\,sec^{-1}$
μ_{max}	1360	495	$cm^2\,V^{-1}\,sec^{-1}$
N_{ref}	1.3×10^{17}	6.3×10^{16}	cm^{-3}
α	0.91	0.76	—

The dashed line in Fig. 5 represents a fit obtained by Hilsum[54] with the simpler equation:

$$\mu = \frac{\mu_{max}}{1+[N(cm^{-3})/10^{17}]^{1/2}}, \quad (7)$$

which can be obtained from eqn (6) by assuming $\mu_{min} = 0$, $N_{ref} = 10^{17}$ cm^{-3}, $\alpha = 1/2$, and gives a reasonable fit of $\mu(N)$ for electrons in many materials[54].

A third expression for $\mu(N)$ can be obtained as a special case ($E = 0$) of the general formula (see eqn (10)) given by Scharfetter and Gummel[57] for the electric field and impurity dependence of the drift velocity:

$$\mu = \frac{\mu_0}{\sqrt{(1+[N/(N/S+N_{ref})])}} \quad (8)$$

where the parameters have the numerical values given in Table 4. The curves obtained with eqn (8) for electrons and holes are shown in Figs. 5 and 6, respectively, as dot-dashed lines.

Table 4. Best-fitting parameters for the impurity dependence of electron and hole Ohmic mobilities at room temperature, as given in eqn (8), and for the impurity and field dependence of electron- and hole-drift velocities at room temperature, as given in eqn (10)

	Electrons	Holes	Units
μ_0	1400	480	cm^2 V^{-1} sec^{-1}
N_{ref}	3×10^{16}	4×10^{16}	cm^{-3}
S	350	81	—
A	3.5×10^3	6.1×10^3	V cm^{-1}
F	8.8	1.6	—
B	7.4×10^3	2.5×10^3	V cm^{-1}

5.2 *Drift velocity*

Figures 15 and 16 show the electron and hole drift velocities as functions of the electric field **E** applied along a ⟨111⟩ direction at several temperatures, fitted by the eqn[58, 90]:

$$v_d = v_m \frac{E/E_c}{[1+(E/E_c)^\beta]^{1/\beta}}, \quad (9)$$

the values and temperature dependences ($T \geq 250$ K) of the parameters v_m, E_c, and β being given in Table 5[90].

Scharfetter and Gummel[57] have given the following phenomenological expression for drift velocity, for both

Table 5. Best-fitting parameters for the electric field and temperature dependence of electron and hole drift velocities in high-purity silicon, as given in eqn (9)

	Electrons	Holes	Units
v_m	$1.53\times10^9\times T^{-0.87}$	$1.62\times10^8\times T^{-0.52}$	cm sec^{-1}
E_c	$1.01\times T^{1.55}$	$1.24\times T^{1.68}$	V cm^{-1}
β	$2.57\times10^{-2}\times T^{0.66}$	$0.46\times T^{0.17}$	—

T is measured in degrees Kelvin

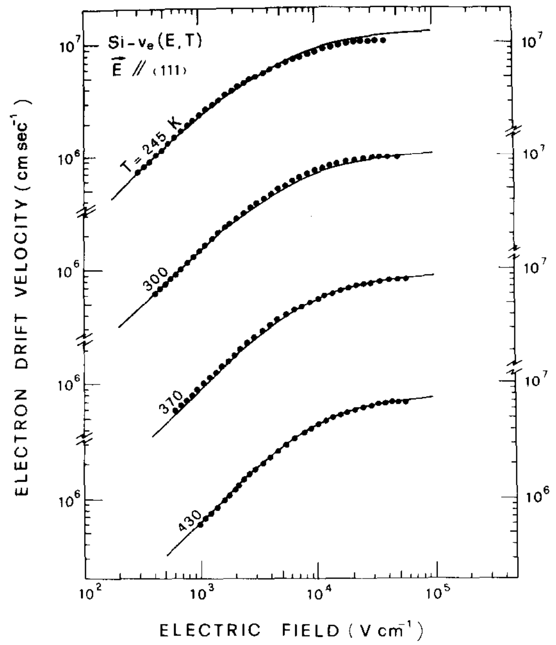

Fig. 15. Electron drift velocity in high-purity silicon[28, 90] for $E\|\langle111\rangle$ as a function of the electric field at four different temperatures. The points represent the experimental data[90] and the continuous lines are the best-fitting curves obtained with eqn (9) using the parameters listed in Table 5.

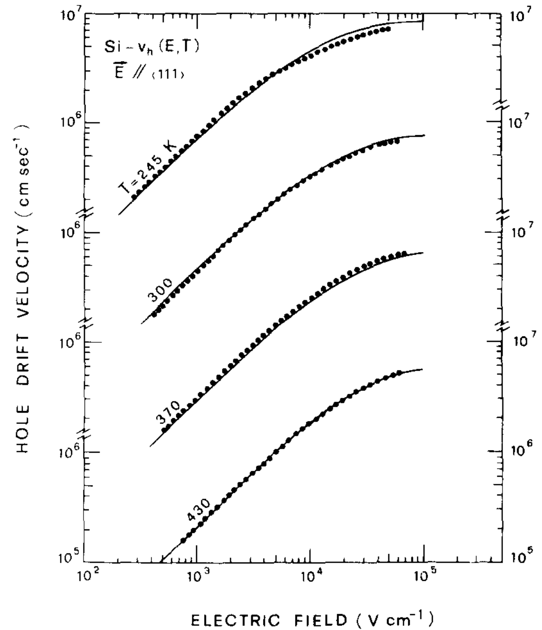

Fig. 16. Hole drift velocity in high-purity silicon[28, 90] for $E\|\langle111\rangle$ as a function of the electric field at four different temperatures. The points represent the experimental data[90] and the continuous lines are the best fitting curves obtained with eqn (9) using the parameters listed in Table 5.

electrons and holes, as a function of impurity concentration and electric field at room temperature:

$$v_d = \frac{\mu_0 E}{\left\{1+\frac{N}{N/S+N_{ref}}+\frac{(E/A)^2}{E/A+F}+\left(\frac{E}{B}\right)^2\right\}^{1/2}} \quad (10)$$

The values of the parameters are reported in Table 4. As we have seen above, eqn (10) gives a good fit of the experimental Ohmic mobility versus impurity concentration. In Fig. 17, where eqn (10) is plotted for different N, it is shown that it also gives a good representation of the high-field drift velocity of electrons in pure materials. Since, to the authors knowledge, experimental data of high-field v_d in doped silicon are not available, we cannot check the validity of eqn (10) in this case, even though all the boundary conditions seem to suggest that it should not be far from the real values of v_d. The same considerations, relative to eqn (10), are also valid for holes. Another expression for drift velocity as a function of N and E at room temperature can be obtained by combining eqns (6) and (9), with $E_c = v_m/\mu$.

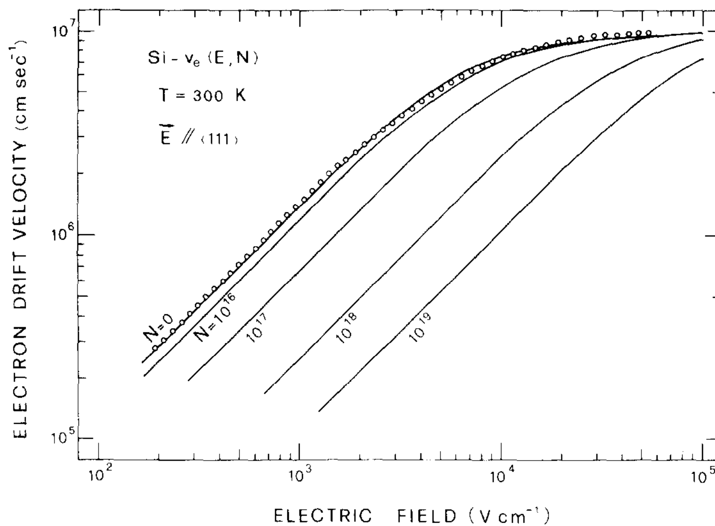

Fig. 17. Electron drift velocity at room temperature as a function of impurity concentration and of field strength obtained with eqn (10). Open points are the experimental results for high-purity material [28] reported in Fig. 7.

5.3 *Saturation drift velocity*

We found that the experimental data of electron "saturated" (see Section 4.3) drift velocity as a function of temperature given in Fig. 11, can be represented by the equation (continuous line in the figure):

$$v_s = \frac{v^*}{1 + C\exp(T/\Theta)}, \quad (11)$$

where $v^* = 2.4 \times 10^7$ cm sec^{-1}, $C = 0.8$ and $\Theta = 600$ K.

6. CONCLUSIONS

The basic transport properties of charge carriers in silicon have been reviewed in this paper. The knowledge of the fundamental microscopic processes which determine these transport properties in bulk material is today rather satisfactory, especially as regards electrons, thanks to the availability of high purity material or of material with controlled doping, and to the recent formulation of powerful numerical methods to solve the transport equation. In order to complete the picture presented in this review, a detailed experimental analysis of the effect of impurities on high-field transport, for both electrons and holes, needs to be undertaken. Were these data available, they could lead to a general phenomenological equation of drift velocity as a function of temperature, field and impurity content, which would be of particular interest in device modelling.

Further theoretical and experimental investigations into the field-dependence of the diffusion coefficients of both electrons and holes also need to be performed, for data are still scarce and imprecise. These investigations should be linked with the study of hot-electron noise, since the correlation between diffusion and noise, out of thermal equilibrium, still seems to be an intriguing problem.

Finally, while bulk transport, as stated above, is fairly well understood, an equally satisfactory understanding of surface transport, would still appear to be lacking.

Acknowledgements—We are grateful to Drs. G. Baccarani and L. Reggiani for many useful discussions, and to Drs. J. P. Nougier and M. Rolland for providing unpublished data.

In particular, we should like to thank Prof. M. A. Nicolet, who first suggested the usefulness of a review of this type and whose advice in its realization was most appreciated.

REFERENCES

1. J. M. Ziman, *Electrons and Phonons*, (Edited by N. F. Mott, E. C. Bullard and D. H. Wilkinson). Oxford University Press, London (1960).
2. R. A. Smith, *Semiconductors*. Cambridge University Press (1959).
3. P. N. Butcher, *Electrons in Crystalline Solids*. IAEA, Vienna, *STI/PUB*/335, p. 103 (1973).
4. W. Fawcett, *Electrons in Crystalline Solids*. IAEA, Vienna, STI/PUB/335, p. 531 (1973).
5. E. M. Conwell, *High Field Transport in Semiconductors* (Edited by F. Seitz and D. Turnbull), Solid State Physics, Suppl. 9. Academic, New York (1967).
6. J. R. Chelikowsky and M. L. Cohen, *Phys. Rev.* **B10**, 5095 (1974).
7. J. C. Hensel, H. Hasegawa and N. Nakayama, *Phys. Rev.* **138**, A225 (1965).
8. C. Canali, C. Jacoboni, F. Nava, G. Ottaviani and A. Alberigi Quaranta, *Phys. Rev.* **B12**, 2265 (1975).

9. G. Dresselhaus, A. F. Kip and C. Kittel, *Phys. Rev.* **131**, 2242 (1963).
10. O. Kane, *J. Phys. Chem. Solids* **1**, 82 (1965).
11. G. Ottaviani, L. Reggiani, C. Canali, F. Nava and A. Alberigi Quaranta, *Phys. Rev.* **B12**, 3315 (1975).
12. H. D. Rees, *J. Phys. C: Solid State Physics* **5**, 641 (1972).
13. W. Fawcett, A. D. Boardman and S. Swain, *J. Phys. Chem. Solids* **31**, 1963 (1970).
14. C. Hammar, *J. Phys. C: Solid State Physics* **6**, 70 (1973).
15. J. R. Haynes and W. Shockley, *Phys. Rev.* **75**, 691 (1949); *Phys. Rev.* **81**, 835 (1951).
16. E. J. Ryder and W. Shockley, *Phys. Rev.* **81**, 139 (1951).
17. W. Shockley, *Bell. System Tech. J.* **30**, 990 (1951).
18. E. J. Ryder, *Phys. Rev.* **90**, 766 (1953).
19. A. C. Prior, *J. Phys. Chem. Solids* **12**, 175 (1959).
20. K. Seeger, *Phys. Rev.* **114**, 476 (1959).
21. J. Zucker, V. J. Fowler and E. M. Conwell, *J. Appl. Phys.* **32**, 2606 (1961).
22. A. F. Gibson, J. W. Granville and E. G. S. Paige, *J. Phys. Chem. Solids* **19**, 198 (1961).
23. M. A. C. S. Brown, *J. Phys. Chem. Solids* **19**, 218 (1961).
24. C. Hamaguchi and Y. Inuishi, *J. Phys. Chem. Solids* **27**, 1511 (1966).
25. W. E. Spear, *J. Phys. Chem. Solids* **21**, 110 (1961).
26. C. B. Norris and J. F. Gibbons, *IEEE Trans. Electron Devices* **ED-14**, 30 (1967).
27. J. G. Ruch and G. S. Kino, *Phys. Rev.* **174**, 174 (1968).
28. C. Canali, G. Ottaviani and A. Alberigi Quaranta, *J. Phys. Chem. Solids* **32**, 1707 (1971).
29. M. Martini, J. W. Mayer and K. R. Zanio, *Applied Solid State Science* (Edited by R. Wolfe), Vol. 3. Academic, New York (1972).
30. T. W. Sigmon and J. F. Gibbons, *Appl. Phys. Lett.* **15**, 320 (1969).
31. C. Canali, C. Jacoboni, G. Ottaviani and A. Alberigi Quaranta, *Appl. Phys. Lett.* **27**, 278 (1975).
32. J. P. Nougier and M. Rolland, *Phys. Rev.* **B8**, 5728 (1973).
33. M. Rolland, Thesis, and M. Rolland and J. P. Nougier, private communication.
34. G. Persky and D. J. Bartelink, *J. Appl. Phys.* **42**, 4414 (1971).
35. V. Rodriguez, H. Ruegg and M-A. Nicolet, *IEEE Trans. Electron Devices* **ED-14**, 44 (1967).
36. V. Rodriguez and M-A. Nicolet, *J. Appl. Phys.* **40**, 496 (1969).
37. T. E. Seidel and D. L. Scharfetter, *J. Phys. Chem. Solids* **28**, 2563 (1967).
38. C. Y. Duh and J. L. Moll, *IEEE Trans. Electron Devices* **ED-14**, 46 (1967); *Solid-St. Electron.* **11**, 917 (1968).
39. G. A. Acket and J. de Groot, *IEEE Trans. Electron Devices* **ED-14**, 505 (1967).
40. W. Einle, *Electron. Lett.* **3**, 52 (1967).
41. B. L. Boichenko and V. M. Vasetskii, *Soviet Phys. Solid State* **7**, 1631 (1966).
42. M. H. Jørgensen, N. I. Meyer and K. J. Schmidt-Tiedeman, *Proc. VII Internat. Conf. Phys. Semicond.*, Paris, p. 457 (1964).
43. M. Asche, B. L. Boichenko and O. G. Sarbej, *Phys. Stat. Sol.* **9**, 323 (1965).
44. J. G. Nash and J. W. Holm-Kennedy, *Appl. Phys. Lett.* **24**, 139 (1974); Appl. Phys. Lett. **25**, 507 (1974).
45. P. J. Price, *Fluctuation Phenomena in Solids* (Edited by R. E. Burgess). Academic, New York (1965).
46. J. C. Portal, L. Eaves, S. Askenazy and R. A. Stradling, *Solid State Commun.* **14**, 1241 (1974); and *Proc. 12th Int. Conf. Physics of Semiconductors* (Edited by M. H. Pilkum). Teubner, Stuttgart (1974).
47. C. Jacoboni, R. Minder and G. Majni, *J. Phys. Chem. Solids* **36**, 1129 (1975); M. Costato and L. Reggiani, *Lett. Nuovo Cimento* **3**, 728 (1970).
48. G. Gagliani and L. Reggiani, *Nuovo Cimento* **30B**, 207 (1975).
49. P. Norton, T. Braggins and H. Levinstein, *Phys. Rev.* **B8**, 5632 (1973).
50. F. J. Morin and J. P. Maita, *Phys. Rev.* **96**, 28 (1954).
51. L. Gherardi, A. Pellacani and C. Jacoboni, *Lett. Nuovo Cimento* **14**, 225 (1975).
52. R. A. Logan and A. J. Peters, *J. Appl. Phys.* **31**, 122 (1960).
53. G. Baccarani and P. Ostoja, *Solid-St. Electron.* **18**, 579 (1975).
54. C. Hilsum, *Electron. Lett.* **10**, 259 (1974).
55. J. C. Irvin, *Bell System Tech. J.* **41**, 387 (1962).
56. F. Mousty, P. Ostoja and L. Passari, *J. Appl. Phys.* **45**, 576 (1974).
57. D. L. Scharfetter and H. K. Gummel, *IEEE Trans. Electron Devices* **ED-16**, 64 (1969).
58. D. M. Caughey and R. F. Thomas, *Proc. IEEE* **55**, 2192 (1967).
59. V. I. Fistul, *Heavily Doped Semiconductors.* Plenum, New York (1969).
60. W. Sasaki, M. Shibuya, K. Mizuguchi and G. M. Hatoyama, *J. Phys. Chem. Solids* **8**, 250 (1959).
61. M. Asche and O. G. Sarbej, *Phys. Stat. Sol.* (*a*) **8**, K61 (1971).
62. M. H. Jørgensen, N. O. Gram and N. I. Meyer, *Solid-St. Comm.* **10**, 337 (1972).
63. M. Asche and O. G. Sarbej, *Phys. Stat. Sol.* (*a*) **46**, K121 (1971).
64. N. O. Gram, *Phys. Lett.* **38A**, 235 (1972).
65. C. Canali, A. Loria, F. Nava and G. Ottaviani, *Solid-St. Commun.* **12**, 1017 (1973).
66. J. P. Nougier, M. Rolland and O. Gasquét, *Phys. Rev.* **B11**, 1497 (1975).
67. C. Canali, M. Costato, G. Ottaviani and L. Reggiani, *Phys. Rev. Lett.* **31**, 536 (1973).
68. P. A. Wolff, *Phys. Rev.* **95**, 1415 (1954).
69. D. K. Ferry, *Phys. Rev.* **B12**, 2361 (1975).
70. C. Canali and G. Ottaviani, *Phys. Letters* **32A**, 147 (1970).
71. L. Reggiani, G. Majni and R. Minder, *Solid-St. Commun.* **16**, 151 (1975).
72. A. F. Gibson, J. W. Granville and E. G. S. Paige, *Proc. V Internat. Conf. Semicond. Prague* p. 112 (1960); *J. Phys. Chem. Solids* **19**, 198 (1961).
73. T. N. Morgan and C. E. Kelly, *Phys. Rev.* **137**, A1537 (1965).
74. K. Hess and K. Seeger, *Z. Physik* **218**, 431 (1968).
75. A. Dargys and T. Banys, *Phys. Stat. Solidi* **52b**, 699 (1972).
76. G. Baccarani, C. Jacoboni and A. M. Mazzone, *Solid-St. Electron.* **20**, 5 (1977).
77. F. Nava, private communication.
78. J. R. Schrieffer, *Phys. Rev.* **97**, 641 (1955).
79. R. F. Pierret and C. T. Sah, *Solid-St. Electron.* **11**, 279 (1968).
80. F. Stern, CRC Crit. *Rev. Solid State Sci.* **4**, 499 (1974).
81. F. Stern and W. S. Howard, *Phys. Rev.* **163**, 816 (1967).
82. N. St. J. Murphy, F. Berz and I. Flinn, *Solid-St. Electron.* **12**, 775 (1969).
83. O. Leistiko and A. S. Grove, *IEEE Trans. Electron Devices* **ED-12**, 248 (1965).
84. F. F. Fang and A. B. Fowler, *Phys. Rev.* **169**, 619 (1968).
85. K. Hess and C. T. Sah, *J. Appl. Phys.* **45**, 1254 (1974).
86. T. Sato, Y. Takeishi, H. Hara, Y. Okamoto, *Phys. Rev.* **B4**, 1950 (1971).
87. F. F. Fang and A. B. Fowler, *J. Appl. Phys.* **41**, 1825 (1970).
88. T. Sato, Y. Takeishi, H. Tango, H. Ohnuma and Y. Okamoto, *J. Phys. Soc. Japan* **31**, 1846 (1971).
89. H. Sasaki and T. Sugano, *J. Jap. Soc. Appl. Phys. Suppl.* **41**, 141 (1972).
90. C. Canali, G. Majni, R. Minder and G. Ottaviani, *IEEE Trans. Electron Devices* **ED-22**, 1045 (1975).
91. S. Denda and M-A. Nicolet, *J. Appl. Phys.* **37**, 2412 (1966).
92. G. Baum and H. Beneking, *IEEE Trans. Electron Devices* **ED-17**, 481 (1970).
93. F. N. Trofimenkoff, *Proc. IEEE* **53**, 1765 (1965).